Potential Low Bias in High-Wind Drag Coefficient Inferred from Dropsonde Data in Hurricanes

David H. Richter,[a] Charlotte Wainwright,[a] Daniel P. Stern,[b] George H. Bryan,[c] and
Daniel Chavas[d]

[a] *Department of Civil and Environmental Engineering and Earth Sciences, University of Notre Dame, Notre Dame, Indiana*
[b] *University Corporation for Atmospheric Research, Monterey, California*
[c] *National Center for Atmospheric Research, Boulder, Colorado*
[d] *Department of Earth, Atmospheric, and Planetary Sciences, Purdue University, West Lafayette, Indiana*

ABSTRACT: Understanding momentum exchange at the air–sea interface is important for accurate hurricane predictions and understanding fundamental storm dynamics. One method for estimating air–sea momentum transfer in high winds is the flux-profile method, which infers surface momentum fluxes and the corresponding drag coefficient from mean velocity profiles obtained from either dropsondes or meteorological towers, under the assumption that the boundary layer wind profile at low altitudes exhibits a logarithmic profile with height. In this study, we use dropsonde data from reconnaissance aircraft, as well as "virtual sondes" from a turbulence-resolving simulation of an intense tropical cyclone, to critically analyze the diagnosis of drag coefficient C_D at hurricane-force wind speeds. In particular, the "rolloff" of the drag coefficient, where C_D decreases at 10-m wind speeds > 35 m s^{-1}, is called into question based on uncertainty due to relatively low sample size and a lack of robustness of the flux-profile method at high winds. In addition, multiple factors appear to favor an underestimate of C_D at hurricane-force winds relative to their true values, including uncertainty in the height of recorded dropsonde data, in violation of Monin–Obukhov similarity theory near the eyewall, and the short vertical extent of the logarithmic layer. Due to these and other related sources of uncertainty, it is likely that a quantitative limit has been reached in inferring the specific values of u_* and C_D using the flux-profile method, while at the same time the potential for underestimation may cast doubt on the C_D–U_{10} relationship inferred from this method at high winds.

KEYWORDS: Air–sea interaction; Hurricanes/typhoons; Dropsondes

1. Introduction

While the topic of air–sea exchange has been the subject of research for decades (Large and Pond 1981), hazardous conditions and practical difficulties impede our understanding of the relevant processes at high winds. In particular, it is well known that the bulk coefficients of momentum and enthalpy transfer (C_D and C_K, respectively) are crucial for obtaining accurate intensity forecasts of tropical cyclones (Emanuel 1995; Montgomery et al. 2010; Bryan 2012; Green and Zhang 2014). Existing theory for the maximum potential intensity in a tropical cyclone (Emanuel 1986, 1995), as well as changes in intensity (Tang and Emanuel 2012; Emanuel 2012) depend explicitly on the ratio of these coefficients. However, our ability to measure these values in situ remains restricted primarily to indirect estimates (Jarosz et al. 2007; Bell et al. 2012) or limited/incomplete sets of direct observations (French et al. 2007; Bi et al. 2015; Voermans et al. 2019). Furthermore, influences such as the effects of sea spray (Andreas et al. 1995; Veron 2015; Richter and Stern 2014) and waves (Holthuijsen et al. 2012, hereafter H12; Takagaki et al. 2012; Kudryavtsev et al. 2014) remain difficult to describe and evaluate at high winds, and models developed to predict these effects suffer from a high degree of uncertainty. Parameterizations of C_D and C_K which attempt to include effects of spray and/or waves, for example, have a strong impact on tropical cyclone predictions (Andreas and Emanuel 2001; Wang et al. 2001; Bao et al. 2011),

emphasizing the need for better understanding the physics behind heat and momentum transfer at the air–sea interface.

In one of the earliest attempts to estimate C_D within tropical cyclones, Powell et al. (2003, hereafter P03) used dropsondes to construct mean velocity profiles, and from these, surface stresses (and thus C_D) were calculated using Monin–Obukhov similarity theory relating the logarithmic profile of mean winds to the friction velocity u_*. In their study, P03 found that the drag coefficient appears to peak around a 10-m wind speed of 38 m s^{-1}, followed by a decrease at still higher winds. Around the same time, however, the laboratory measurements of Donelan et al. (2004) (since corrected by Curcic and Haus 2020) seemed to indicate that C_D indeed stops increasing around the same wind speed, but saturates to a constant value instead of bending downward.[1] This is a feature seen in other laboratory experiments as well: Takagaki et al. (2012) and Komori et al. (2018) report a similar saturation at nearly the same wind speed, as do the measurements of Troitskaya et al. (2012, 2020). Since laboratory experiments are limited to very young waves, it is not clear whether the saturation behavior seen in the experiments (and not seen in the observations of P03) should be directly observed in the hurricane boundary layer, or whether properties such as wind–wave alignment fundamentally change this (see H12).

---

[1] The new C_D values of Curcic and Haus (2020) are systematically higher than those reported in Donelan et al. (2004), but still saturate.

In terms of the high-wind saturation behavior, other estimates of C_D at tropical cyclone wind speeds are inconclusive. The aircraft measurements from the Coupled Boundary Layers Air–Sea Transfer (CBLAST) campaign calculated stress using direct eddy covariance (Black et al. 2007; French et al. 2007), but only up to 10-m wind speeds of roughly $30\,\mathrm{m\,s^{-1}}$. Over the range of their measurements, C_D matched reasonably well with other estimates, including those of P03. The same can be said for the eddy covariance measurements of Bi et al. (2015), taken from two coastal towers in the South China Sea. From buoy-based eddy covariance measurements, Potter et al. (2015) observed a slight rolloff of C_D, but at a significantly lower wind speed ($\approx 22\,\mathrm{m\,s^{-1}}$). Their values of C_D lie in the range of other measurements, and they suggest that waves play a role in the observed C_D dependence on wind speed. The momentum budget estimates of Bell et al. (2012) provide C_D out to very high winds (10-m wind speeds above $70\,\mathrm{m\,s^{-1}}$), but the large inherent uncertainty in these approximations precludes any definitive conclusion about even the slope of C_D versus wind speed beyond $40\,\mathrm{m\,s^{-1}}$, let alone its precise value. The direct aircraft measurements of Sparks et al. (2019) and Zhao et al. (2020) made in Pacific typhoons suggest that the momentum flux changes with wind speed in a way consistent with a saturation of C_D; however, while extending out to $60\,\mathrm{m\,s^{-1}}$, the measurements are again quite uncertain. Likewise, other direct measurements of boundary layer turbulence in tropical cyclones, namely, those of Zhang et al. (2011a), are also uncertain and scarce in sample size. Finally, new technologies for measuring momentum fluxes using unmanned aircraft are emerging, and recent prototype measurements show promise for making direct eddy covariance measurements near the eyewall and within the boundary layer, for sustained periods of time (Cione et al. 2020). These have not yet matured, however, to the point of refining the relationship of C_D with wind speed.

Meanwhile, estimates of C_D have also been made from the ocean side in perhaps the only other studies which corroborate the nonmonotonic behavior of C_D with wind speed (aside from H12, which is an extension of P03). Jarosz et al. (2007) uses an upper-ocean momentum balance to show that C_D may peak around $35\,\mathrm{m\,s^{-1}}$ and decrease at higher wind speeds. Similar approaches were used also by Sanford et al. (2011) and Hsu et al. (2017), but the overall behavior is both quantitatively and qualitatively different between the three ocean mixed layer studies. Sanford et al. (2011) appears to underestimate C_D relative to other studies at most wind speeds, while Hsu et al. (2017) appears to overestimate, albeit with a peak around $30\,\mathrm{m\,s^{-1}}$ and a decrease beyond. More recently, Hsu et al. (2019) expanded the work of Hsu et al. (2017) to additional storms, and noted the impacts of both wind-wave alignment and storm speed on the C_D estimates. However, once again, when considering the variability between ocean-based estimates, even a clear qualitative behavior of C_D is unavailable at winds beyond roughly $30\,\mathrm{m\,s^{-1}}$.

In this study, we focus exclusively on the flux-profile method employed by P03 and H12 in order to revisit their estimation of the high-wind behavior of C_D and explore the potential for its underestimation. In a previous study, Richter et al. (2016) evaluated the flux-profile method and quantified the uncertainty of the resulting C_D (and C_K) based on both methodological choices (e.g., sonde binning strategy, height over which profiles were fit) and measurement uncertainty (e.g., confidence bounds of the computed mean velocity at each height). For the flux-profile method, it was found that values of C_D were subject to at least 50% uncertainty out to $50\,\mathrm{m\,s^{-1}}$, with even higher uncertainty at higher winds. Furthermore, this uncertainty was caused by multiple influences (including those listed above), calling into question whether or not these estimates could be refined further, even given more data. Richter et al. (2016) also performed a preliminary analysis of the flux-profile method on artificial "virtual sondes" computed within a turbulence-resolving tropical cyclone simulation (Stern and Bryan 2018), and by comparing to the known, prescribed surface flux coefficients, found that virtual sondes near the radius of maximum winds (RMW) appear to underestimate the true values of C_D. A similar strategy is employed in the current study.

It is well understood that near the eyewall of a tropical cyclone, boundary layer dynamics depart significantly from standard geostrophic, horizontally homogeneous conditions due to strong radial pressure gradients, convective updrafts, and secondary circulations (Smith 1968; Kepert 2001; Foster 2009). Even the term "boundary layer" can refer to different physical heights (Zhang et al. 2011b). As a result, the existence of a logarithmic layer over which to apply the flux-profile method has been called into question in this region (Smith and Montgomery 2014), although standard theory does not necessarily preclude (or affirm) its presence (Tennekes 1973).

Since the eyewall region is typically where the highest wind speeds are found, the objective of this study is therefore to evaluate the possibility that high-wind estimates of C_D using the flux-profile method can yield inaccurate values, even for the basic qualitative question of whether C_D has a nonmonotonic relationship with wind speed. Indeed, Vickery et al. (2009), who built on the work of P03 using the same technique, suggested that the nonmonotonic behavior of C_D may disappear when considering only dropsondes from outside the RMW. To carry out this work, we employ and analyze the virtual sondes of Stern and Bryan (2018) as well as dropsonde data from a large number of storms, including recent data from updated dropsonde hardware and software, and assess the reliability of the flux-profile method and gauge its dependence on storm-relative location (among other factors). This study extends this type of analysis in order to highlight the potential for underestimating C_D near the RMW and thus at high winds.

2. Method

a. Dropsonde data

GPS dropsonde data used here were downloaded from the publicly available dataset released by the National Oceanic and Atmospheric Administration (NOAA) Hurricane Research Division (HRD). The dropsonde data were collected by NOAA research and Air Force reconnaissance aircraft from storms in the Atlantic and east Pacific basins and span the

period 1997–2018. The raw dropsonde data are quality controlled via either the Editsonde software from HRD or Atmospheric Sounding Processing Environment (ASPEN) software from the National Center for Atmospheric Research (NCAR).

The aircraft generally fly at heights between 1.5 and 4 km, and once a sonde is launched it falls vertically while being advected horizontally by the wind. The sonde fall speed is approximately 10–12 m s^{-1} in the lower troposphere, and sondes take an average of 3–6 min to reach the ocean surface. Prior to 2010, pressure, temperature, and humidity, and wind speed and direction were measured at 2-Hz frequency. In 2010 the dropsondes were updated and the frequency of wind measurements was increased to 4 Hz, with other measurements remaining at 2 Hz (Wang et al. 2015). Since the geopotential height is based on the 2-Hz pressure sampling, this results in the wind data height resolution of approximately 8 m across the dataset. The dropsonde data used herein encompass those used in the analyses of both P03 and Richter et al. (2016) and are updated to include storms up to 2018.

Within the analysis, the sondes are binned based on the radial location of the sonde relative to the RMW. The radial distance of each sonde from the storm center is evaluated using the HRD track files, which provide the latitude and longitude of the storm center at 2-min intervals based on the method of Willoughby and Chelmow (1982). The RMW is taken from one of two datasets: TC-OBS (Vigh et al. 2020), version 0.40, which includes data from all dropsondes from NOAA and USAF flights between 1989 and 2015 sampling Atlantic storms, and the extended best track (EBT) dataset (Demuth et al. 2006), which includes data from the Atlantic basin spanning 1988–2018 and the eastern North Pacific basin spanning 2001–18. The TC-OBS data provide the radius and speed of the maximum winds at 1-h intervals, while the EBT data provide these at 6-h intervals. In our analysis, the RMW is taken from the TC-OBS data where available, due to the higher-frequency update time this provides, and the EBT data are used for all storms not contained in the TC-OBS dataset. For each individual dropsonde, the time of the sonde drop is compared to those from the track data, TC-OBS, and EBT, to find the corresponding location of the storm center and the RMW at that time. The RMW is compared to the radial distance of the sonde drop from the storm center to give the sonde radial distance as a fraction of RMW (hereafter R/RMW).

To estimate C_D based on dropsonde data, we employ the flux-profile method, as in P03, H12, and Richter et al. (2016). This method is based on the construction of mean logarithmic wind profiles within the hurricane boundary layer. According to Monin–Obukhov similarity theory, in a neutrally stable boundary layer where small-scale surface effects, including the effects of surface currents, are negligible, the mean velocity profile can be described by

$$\langle u \rangle = \frac{u_*}{\kappa} \ln \left(\frac{z}{z_0} \right), \tag{1}$$

where $\langle \cdot \rangle$ represents ensemble averaging, u_* is the friction velocity, κ is the von Kármán constant, which is taken here to be 0.4, z_0 is the roughness length, and z is height above the

surface. The friction velocity is defined as a function of the total surface stress τ_w and air density ρ via

$$\rho u_*^2 = \tau_w. \tag{2}$$

Parameterizations for surface stress are formulated based upon conditions at a reference height, usually taken as 10 m (so U_{10} is the mean 10-m wind speed), and defined in terms of a drag coefficient C_D:

$$\tau_w = \rho u_*^2 = \rho C_D U_{10}^2. \tag{3}$$

A mean logarithmic wind profile [Eq. (1)] is then constructed, and when $\langle u \rangle$ is plotted against $\ln(z)$, the best-fit line has a slope m which is equal to κ/u_*, and an intercept which is a function of the roughness length z_0. Once the slope m is known, U_{10} can be evaluated by setting z as 10 m in Eq. (1), and C_D can then be calculated by rearranging Eq. (3):

$$C_D = \frac{u_*^2}{U_{10}^2} = \frac{\kappa^2}{m^2 U_{10}^2}. \tag{4}$$

To examine C_D as a function of U_{10}, the sondes are split into bins depending on the mean wind speed (U_{mean}) recorded between the surface and a given height H_{mean}. The mean wind speed across all profiles within that bin of width ΔU_{bin} is evaluated at height intervals Δz_{bin} within a height range bounded by z_{max} and z_{min}.

The sensitivity of the flux-profile method to the choices of H_{mean}, ΔU_{bin}, Δz_{bin}, z_{max}, and z_{min} was investigated by Richter et al. (2016), who found that the choice of fitting parameters can produce C_D estimates which vary by up to 50%. This uncertainty in the estimated C_D was highest at high wind speeds, as the amount of sonde data available decreases sharply with increasing wind speed. For the analysis presented herein, the values of several of the fitting parameters are selected to match those of P03 to facilitate comparison with their results. We set $H_{mean} = 500$ m, $\Delta z_{bin} = 10$ m, $z_{min} = 10$ m, and $z_{max} = 150$ m. The value of ΔU_{bin} is set as 10 m s^{-1} and the profiles are evaluated over a wind speed range from $U_{mean} = 10$ to 70 m s^{-1}. All profiles with $U_{mean} > 70$ m s^{-1} are grouped into a single bin due to the relatively small number of profiles with such high wind speeds.

A total of 11 939 sondes are available from NOAA HRD. Our analysis removes those which have an R/RMW value greater than 10, those which do not have any data available below a height of 150 m, and those with $U_{mean} < 10$ m s^{-1}. After filtering, 5489 sondes are left that meet these criteria. These remaining sondes are used to evaluate C_D as a function of U_{10}, and to investigate the dependence of C_D on the radial distance from the storm center.

b. Simulation data

To further examine the performance of the flux-profile method for calculating C_D in high winds, we test the method on simulation output of an idealized tropical cyclone. The cyclone is simulated using Cloud Model 1 (CM1; Bryan and Fritsch 2002; Bryan and Morrison 2012).

A fine mesh is used over the central region of interest (80 km × 80 km) with horizontal grid spacing of 31.25 m. Beyond this region the horizontal grid spacing increases with radial distance to a maximum of 15 km at the outer edge of the domain. The vertical grid spacing in the lowest 3 km is 15.625 m. Above 3 km it gradually increases to 500 m at a height of 8 km, and remains at 500 m until the model top is reached at 25 km. Full details of the large-eddy simulation (LES) setup used for this case can be found in Stern and Bryan (2018). Of particular relevance is the surface stress parameterization scheme. C_D is equal to 1×10^{-3} when the 10-m wind speed (U_{10}) is 5 m s^{-1} or below, and increases linearly to a value of 2.4×10^{-3} as U_{10} reaches 25 m s^{-1}. For $U_{10} > 25 \text{ m s}^{-1}$, C_D remains at a constant value of 2.4×10^{-3}.

Virtual dropsonde trajectories are constructed from the simulation output, tracing the path that a dropsonde released into the simulated cyclone would have taken as it is advected by the wind over time. The method of using virtual dropsondes based on CM1 output to examine storm dynamics and investigate uncertainty in the flux-profile method has previously been employed by Richter et al. (2016) and Stern and Bryan (2018). Since the LES code prescribes a value for C_D in the surface flux parameterization as described above, by applying the method outlined in section 2a to the simulated dropsonde data, we can test how well the flux-profile method performs at retrieving a known value of C_D.

3. Results

a. Real dropsondes

1) FULL DATASET SHOWS SIMILAR BEHAVIOR TO P03 AND H12

To provide context for the average profiles as determined by the observational dropsondes, we construct a height–radius composite of the total wind speed, shown in Fig. 1. We use the same strategy of Zhang et al. (2011b, their Fig. 4), who only incorporate sondes launched while the storm was at least at hurricane strength (in the subsequent analysis, storms of all strengths are considered). As expected, the composite peak winds occur at R/RMW ≈ 1, and are at a height of roughly 500 m at the RMW. The dashed line in Fig. 1 indicates the height of the maximum wind speed at each R/RMW, which has been smoothed using a window average for visualization purposes. The height of the maximum wind decreases with decreasing R/RMW, a feature seen in Zhang et al. (2011b), and as expected from a theoretical perspective (Eliassen 1971; Kepert 2001; Foster 2009). While the composite averaging procedure across so many storms of different intensities can smear out the potentially sharp velocity gradients near the eyewall, Fig. 1 illustrates the overall features of the near-surface wind speed relevant to the analysis which follows.

To begin the process of assessing the surface flux retrieval, we first employ the procedure outlined in section 2 to the entire database of observational dropsondes, without any restriction or strategy beyond binning by the average wind speed in the lowest 500 m—the same strategy employed by P03. Figure 2a shows that when averaging all dropsonde profiles within each
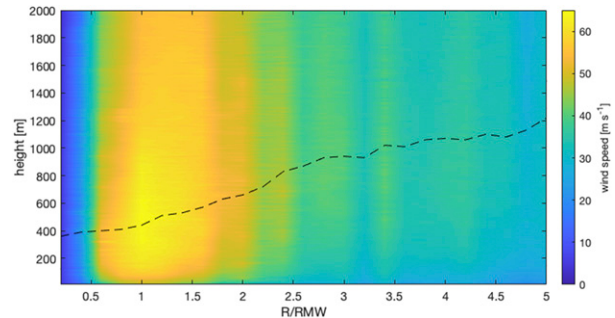

FIG. 1. Mean wind speed magnitude as a function of R/RMW and height from a composite of all observational dropsondes in this study. Sondes are only included for storms of at least hurricane intensity (at the time of the sonde launch). The black dashed line indicates the height of the maximum wind at each R/RMW.

wind speed category, the resulting ensemble mean indeed exhibits a profile with height that strongly resembles a logarithmic layer to a height of at least roughly 150 m. The vertical range over which this is true decreases with increasing boundary layer wind speed, corresponding to the reduction of the height of maximum wind with radius as shown in Fig. 1 and other studies (Zhang et al. 2011b), and the fact that the sondes in the highest few wind speed categories are almost certainly from radii near the RMW. In addition, the height of the maximum wind decreases with intensity, even at the same radius. While some, for example, Smith and Montgomery (2014), question the existence of a logarithmic layer near the RMW, Fig. 2a provides strong evidence that a full ensemble mean does exhibit logarithmic behavior, but only sufficiently below the wind speed maximum [a possibility not excluded by Smith and Montgomery (2014)]. What is not established, however, is whether this apparent logarithmic wind profile is linked to the surface stress in the same way as under the ideal, horizontally homogeneous conditions assumed in the theoretical development of the logarithmic layer (Monin and Yaglom 1971; Tennekes 1973).

If one does assume that standard logarithmic layer theory applies throughout the tropical cyclone surface layer, Figs. 2b and 2c provide the surface friction velocity u_* and drag coefficient C_D as a function of 10-m wind speed. Figure 2c shows that the estimated values of C_D are very close to those provided by P03 and H12, but this is to be expected since it is the same procedure applied to an expanded dataset. The only exception is at the highest wind speeds, where the current C_D estimates do not exhibit as sharp of a drop-off. This difference will be discussed shortly. Similarly, Fig. 2b shows a near-linear increase of u_* with wind speed out to roughly 30 m s^{-1}, beyond which u_* increases more slowly with U_{10}. This change in slope corresponds to the saturation and/or decrease of C_D, resulting from Eq. (4) and discussed in detail by Andreas et al. (2012).

2) SUBDIVIDING SONDE DATASET HIGHLIGHTS LARGE UNCERTAINTY

Since one of the objectives of the present work is to investigate whether the flux-profile method of estimating surface
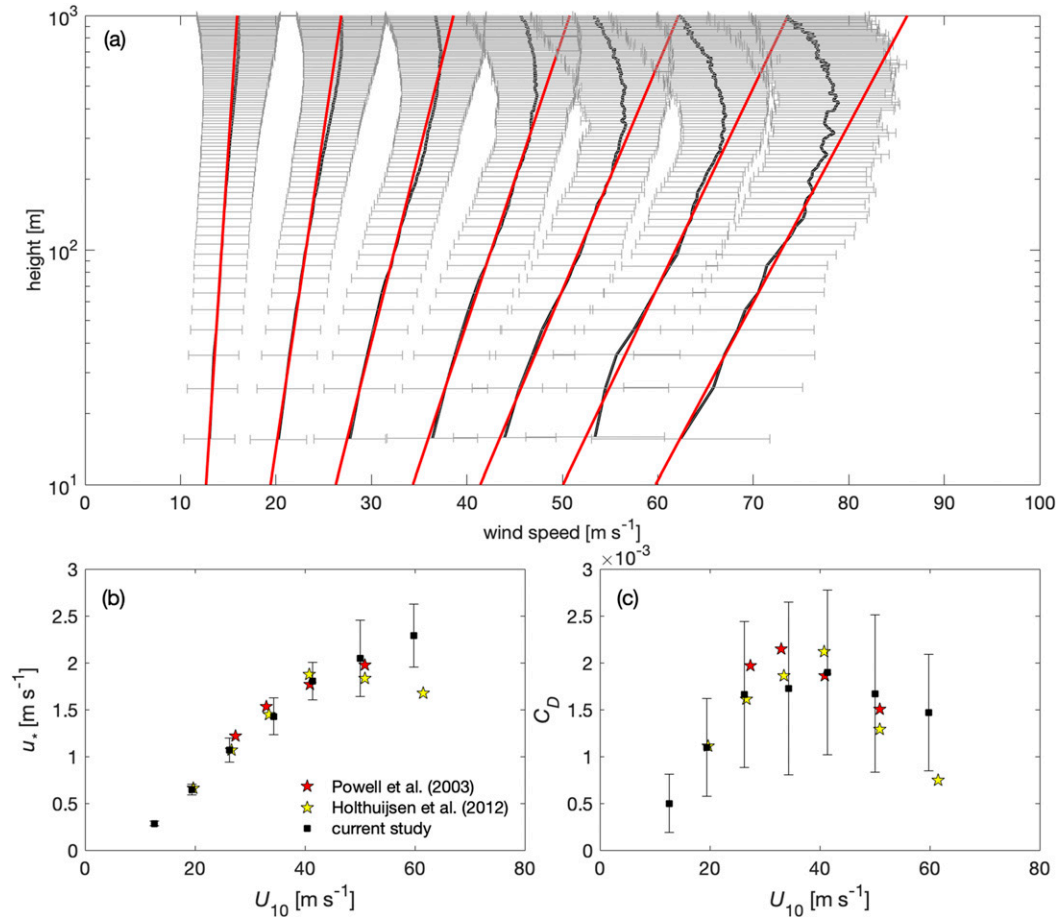
FIG. 2. (a) Mean velocity profiles from all observational sondes included in the analysis. The error bars represent the 95% confidence interval (CI) based on the mean velocity CI at each height. (b) u_* vs U_{10}. (c) C_D vs U_{10}. The logarithmic profiles are fitted over heights between 10 and 150 m.

fluxes is valid at all storm radii, we repeat the binning, averaging, and fitting procedure, but now as a function of R/RMW. This is done in two ways: first for 8 different bins of R/RMW, ranging between R/RMW = 0 and R/RMW = 10, and second by distinguishing between "near RMW" and "outside RMW," done by separating sondes based on whether they were launched at R/RMW greater or equal to 2. This latter case is reminiscent of the strategy in Vickery et al. (2009).

Figures 3a and 3b show C_D as a function of U_{10} for these two different methods of stratifying by R/RMW. Figure 3a provides the curves for the 8 different ranges of R/RMW, and aside from outliers and noise associated with sample size, there appears to be no systematic dependence of the C_D–U_{10} relationship as a function of normalized radius where the sondes were launched. The caveat, of course, is that beyond roughly $U_{10} \approx 40\,\mathrm{m\,s^{-1}}$, data only exist from sondes launched between $0.5 < R$/RMW < 2.5. Thus, it is not possible to draw any broad conclusions about the dependence of the flux-profile C_D estimate on R/RMW, specifically at high winds, since the highest winds only occur in a narrow range around R/RMW = 1. Likewise, Fig. 3b shows that partitioning by sondes near or outside the

RMW results in C_D estimates which are quantitatively similar in each wind speed range, although the question of whether these values are accurate at high winds remains. When Vickery et al. (2009) performed a similar partition between near and outside the RMW, they noted a lack of rolloff in C_D for sondes taken from sufficiently far from the RMW.

To further emphasize this point, Fig. 3c presents C_D as a function of R/RMW for the sole wind speed bin $30 < U_{\mathrm{mean}} < 40\,\mathrm{m\,s^{-1}}$. Furthermore, individual sondes have also been divided by storm intensity, since it may be postulated that this method should only work for storms of similar intensity. What Fig. 3c demonstrates, however, is that there is again no systematic dependence of C_D on either storm intensity or R/RMW. In fact, the scatter in the C_D estimates is better explained by sample size, which is provided in Fig. 3d. Among radii and storm intensities that have a relatively large number of samples (e.g., category 1 storms near the RMW), there is much less variability in the estimated value of C_D shown in Fig. 3c. However, as stated above, although data points like this may be better statistically converged than others (e.g., category 3 storms near the RMW), this
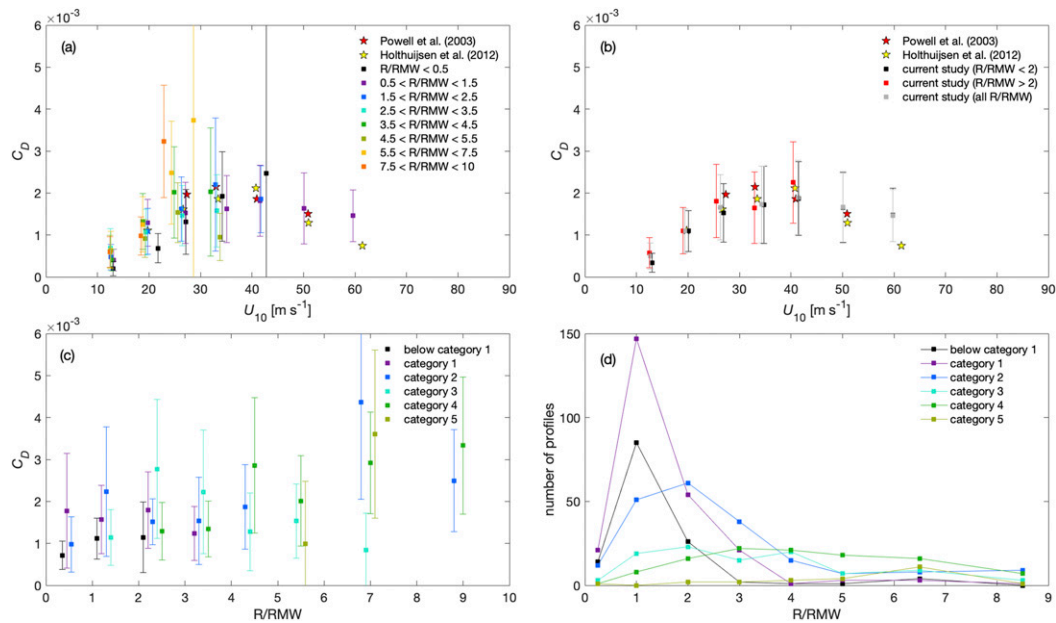
FIG. 3. (a) As in Fig. 2b, but with sondes separated based on R/RMW. (b) As (a), but with an R/RMW separated by a threshold of R/RMW = 2. (c) The dependence of C_D on U_{10} for the wind speed bin $30 < U_{mean} \le 40\,m\,s^{-1}$, separated by storm maximum wind speed at the time of the sonde observations. Slight offsets in R/RMW are included for visual clarity. (d) The number of sondes falling within each storm strength category for the wind speed bin $30 < U_{mean} \le 40\,m\,s^{-1}$.

does not necessarily imply that the quantitative value of C_D is correct.

Next, we revisit the discrepancies between the current estimates and those of P03 and H12 in Figs. 2b and 2c at the highest winds. Figure 4 compares the mean velocity profile and C_D–U_{10} relationship for the same 1997–2005 date range as in H12 versus the result using the date range 2006–18. It is immediately apparent that the qualitative behavior of C_D at high winds is different: using the 1997–2005 range recovers the result of P03 and H12 that C_D peaks and then decreases substantially at the highest winds, while the range 2006–18 actually exhibits a different behavior. The value of C_D at the highest wind speeds exceeds 4×10^{-3}, but is likely influenced by a relatively low sample size at high winds. Regardless, when using the 2006–18 dropsondes one certainly cannot conclude that C_D rolls off as in P03 and H12; rather, these data appear to support a saturation and plateau of C_D at high U_{10}, as in laboratory experiments (e.g., Curcic and Haus 2020). Thus, in Fig. 2, the rolloff of C_D is less pronounced since it includes both date ranges. Once again, we cannot necessarily claim that either is more quantitatively accurate, only that different data yield qualitatively different behaviors at high wind speed. Since it seems highly unlikely that there is a temporal trend in high-wind values of C_D, this result could be a consequence of sample size, or possibly suggests that changes in sonde technology may affect the estimation of C_D.

It is worth noting that the total numbers of sondes in the highest wind speed bins for each of these date ranges is similar. In Fig. 5, a plot of the number of sondes where $U_{mean} > 70\,m\,s^{-1}$ versus year is provided. It is also worth noting that

between the two date ranges being examined, several changes were made to the dropsonde system. First, the GPS receiver was updated in 2005, and the entire software system was upgraded to Airborne Vertical Atmospheric Profiling System (AVAPS) II in 2008. In 2010, the RD-93 sondes were replaced with RD-94, which sampled wind speeds at 4 Hz instead of 2 Hz. While it is coincidental that these changes occur between the date ranges in Fig. 4, it does highlight that the flux-profile method is highly sensitive to sample size, and perhaps can even be influenced by the sampling technology itself. This latter point, however, is merely a hypothesis, and it should be noted that since the pressure (and therefore geopotential height) is still measured at 2 Hz, our mean velocity profiles are effectively sampled at 2 Hz anyway. While changes in sonde software and hardware over the past two decades could in theory have an influence on the measured results, tests performed (not shown) by only analyzing subsets of data from distinct sonde versions or processing software (i.e., Editsonde versus ASPEN), as well as using RMW data from the TC-OBS versus EBT datasets, did not exhibit any conclusive influence. Tests were also conducted by screening sondes by both bathymetric depth and distance to coastline, in the event that shallow water, shoaling waves, or proximity to land could play a role, but again any influence of these factors appears to be minor.

In fact, if one simply takes the entire database of dropsonde measurements and randomly subdivides it, as opposed to subdividing based on date or sonde type, one ultimately encounters the point concluded in Richter et al. (2016): there is simply a large amount of inherent uncertainty in the high-wind behavior of the u_* and C_D estimated from the flux-profile
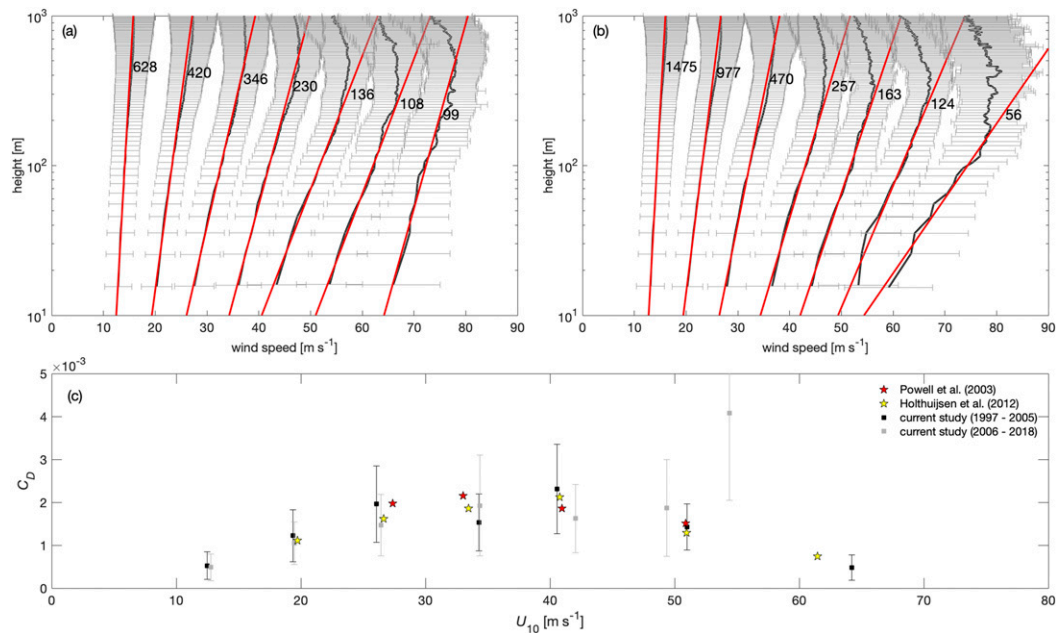
FIG. 4. (a) Mean velocity profiles using data from 1997 to 2005 only, where the values indicate the number of sondes included in each bin. (b) As in (a), but for 2006–18. (c) Retrieved C_D dependence on U_{10} using data from 1997 to 2005 (black) and 2006 to 2018 (gray).

method. While the error bars in figures thus far have represented the 95% confidence interval based on uncertainty of the mean velocity at each height, Figs. 6a and 6b highlight that randomly subsampling the full dropsonde dataset can yield qualitative differences in how C_D and u_*, respectively, behave with wind speed. The green shading is the range over which the estimated values of C_D and u_* are found when splitting the dataset randomly into thirds (this exercise is repeated 20 times), and unsurprisingly, this uncertainty range gets larger at higher winds. Figure 6 would suggest that no conclusion could be drawn even as to the sign of the change in C_D with wind speed above roughly 35 m s^{-1}. This analysis calls into question the notion that C_D decreases at hurricane-strength winds, since this is largely based on the flux-profile results of P03.

3) POSSIBLE LOW BIAS IN THE C_D ESTIMATE

While uncertainty arising from randomly subsampling the full dropsonde dataset demonstrates a large spread in the estimated value of C_D at high winds, we now offer two mechanisms by which the flux-profile method may have a low bias.

The first possible source of bias can result from uncertainty in the vertical position of the sonde just prior to splashdown. While the newer dropsondes have GPS estimates of vertical position, the primary source of vertical height is calculated by integrating the pressure upward from some surface reference, whose value is approximated based on the last recorded pressure reading and an estimate of the splashdown time of the sonde. Because of the fall velocity and data transmission frequency, uncertainty in the $z = 0$ position can be as large as

$O(10)$ m, which at high altitudes is relatively small. Within the lowest 20 m, however, the true vertical position could potentially be off by 100%, altering the mean velocity profile from which to determine u_* in the flux-profile method.

Since there are no data with which to verify the true sonde height at these low elevations, we instead turn to Andreas et al. (2012), who provide a set of independent calculations of u_* and C_D using direct eddy-correlation measurements at relatively lower wind speeds. From multiple datasets, Andreas et al. (2012) show that u_* increases linearly with U_{10}, at least out to roughly 25 m s^{-1} (but the authors speculate that it extends further). Figure 7a provides the empirical fit of
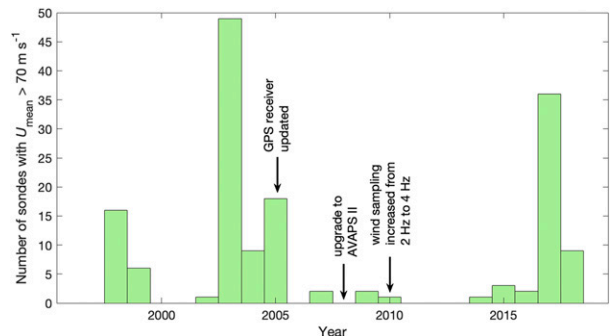

FIG. 5. The number of profiles each year with $U_{mean} > 70$ m s^{-1} included in our analysis. Major upgrades to the dropsonde system are noted.
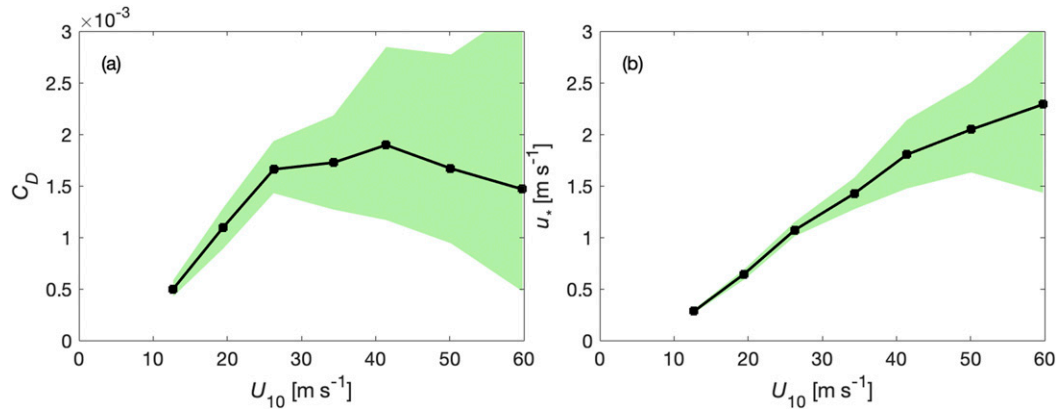
FIG. 6. (a) The black squares show C_D calculated as in Fig. 2a, and the shading represents the variability in C_D when performing 20 repeated tests of randomly subdividing the sonde database into thirds. (b) As in (a), but for u_*.

Andreas et al. (2012) as a solid line, compared to the results of P03, H12, and the current estimates using the full observational dataset. At all wind speeds, the three flux-profile results sit consistently to the right of the solid line, suggesting that the value of u_* is underestimated at each value of U_{10}. We hypothesize that a reasonable explanation for this underestimate is due to the uncertainty of height above the ocean surface: if, for example, one adds a constant 5 m to each sonde measurement (assuming that the true height is actually higher than the recorded height), the gray squares in Fig. 7 shift closer to the solid line, especially for $U_{10} > 25\,\mathrm{m\,s^{-1}}$ (at lower wind speeds, the neglect of stability effects is probably important). While not conclusive, and the 5-m choice here is for representative purposes only, the fact that the flux profile estimates of u_* shift closer to the directly measured values suggests that the uncertainty in sonde height could be an explanatory factor. The resulting values of C_D, shown in Fig. 7b, are then increased, indicating that only a 5 m bias in sonde height could result in a 25% low bias in C_D. Given that waves and swell can exceed 5 m in hurricane conditions, and are not taken into consideration, it certainly seems plausible that this issue could lead to biased estimates of C_D. Furthermore, it is worth noting that Andreas et al. (2012) propose no rolloff

in C_D with wind speed, and instead find that due to the negative intercept of their linear/empirical u_* versus U_{10} relationship, a smooth plateau occurs instead.

The second mechanism which could lead to an underprediction of C_D via the flux-profile method arises when increasing the maximum height of fitting—a choice that is made somewhat arbitrarily and/or subjectively (Richter et al. 2016). For all cases discussed thus far, this has been held fixed at $z_{max} = 150\,\mathrm{m}$. However, based on the shape of the mean velocity profile, in particular due to the peak in wind speed in the range of 300–500 m and the nonmonotonicity of wind speed with height, estimates of u_* decrease with increasing z_{max}, as illustrated in Fig. 8.

In Fig. 8a, the mean velocity profile of all sondes in the range $60 < U_{mean} < 70\,\mathrm{m\,s^{-1}}$ is shown with several colored lines representing fits to different values of z_{max}. Despite the fact that these appear to lie on top of each other, and despite the fact that the R^2 value of the fit exceeds 0.97 for all fits (Fig. 8b), the values of u_* and C_D begin to decrease monotonically once z_{max} exceeds roughly 150 m (Figs. 8c,d). For the case of C_D, these slight variations in the slope lead to decreases of C_D exceeding 10%. Therefore, if the height of maximum wind were lower (e.g., if the mean velocity profile were constructed
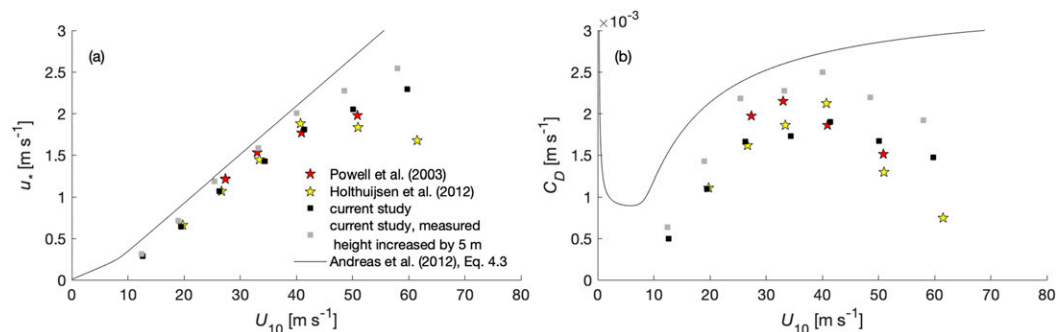

FIG. 7. (a) u_* calculated using the reported sonde height measurements (black squares) and with the sonde height measurements increased by 5 m (gray squares), compared with Eq. (4.3) from Andreas et al. (2012). (b) As in (a), but for C_D.
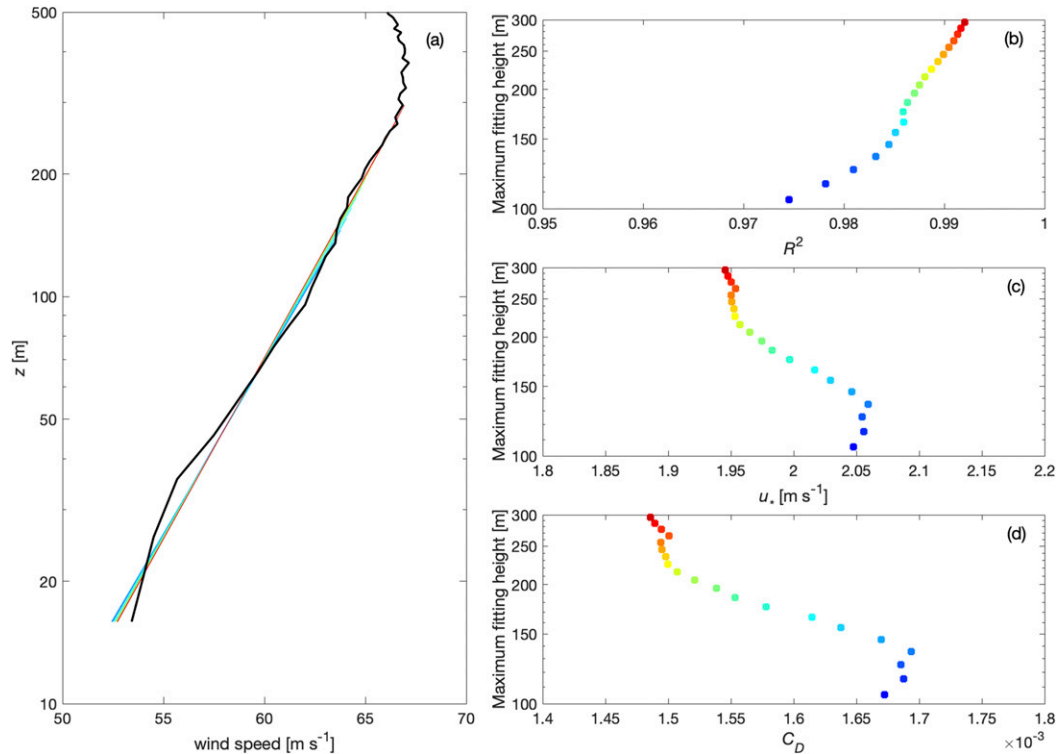
FIG. 8. (a) The black line shows the mean wind profile for the bin $60 < U_{\mathrm{mean}} \leq 70\,\mathrm{m\,s^{-1}}$. The colored lines show the logarithmic fits from 20 m up to various heights. (b) R^2 of the logarithmic fits shown in (a). (c) u_* calculated based on the logarithmic fits shown in (a). (d) C_D calculated using the logarithmic fits shown in (a).

using sondes from a single storm) or a user fitted to a height $z_{\mathrm{max}} > 150\,\mathrm{m}$, seemingly accurate fits of the logarithmic profile could subtly lead to low-biased estimates of C_D. Since the height of maximum wind decreases both with storm radius for a fixed storm and with intensity at a fixed radius, this effect is larger near the RMW and thus at high winds.

b. Virtual dropsondes

From the previous section, we see that the flux-profile method is sensitive to observational sample size, and that even differences in the sign of the C_D–U_{10} relationship at hurricane-force wind speeds cannot be distinguished depending on which date range is included in the analysis. Furthermore, while there appears to be a robust logarithmic layer in mean velocity profiles, no substantive conclusion can be drawn about the reliability of the flux-profile method as a function of R/RMW, and biases may exist which lead to underestimations in C_D, especially at the highest wind speeds. A lack of corroborating data in the high-wind regions precludes a quantitative verification of the values of u_* and C_D obtained in this way.

Therefore, we turn to the virtual sondes described in section 2b, and apply the exact same procedure for estimating u_* and C_D. In this case, the true, prescribed values of both u_* and C_D are known and can be directly compared to the virtual sonde flux-profile estimates. Given that the high grid resolution resolves a substantial portion of the turbulence kinetic energy,

we expect that the surface flux estimates retrieved from the virtual sondes should match the true values in regions where the theory is valid. Note that caution must be used for measurements near the surface where the flow is strongly influenced by the subgrid wall model—we do not use virtual sonde data below $z = 20\,\mathrm{m}$ for this reason. Furthermore, the structure of the simulated storm is small but intense, and not necessarily representative of any one of the storms in the observational dataset; the purpose here is to evaluate the flux-profile method
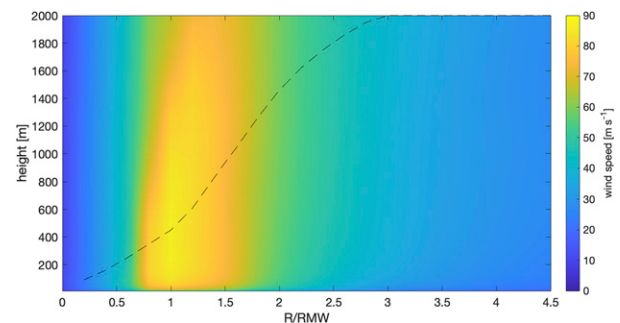

FIG. 9. Mean wind speed as a function of height and R/RMW from the simulated dropsondes. The dashed line indicates the height of maximum winds at each R/RMW bin. Mean wind speeds are calculated based on 10-m height bins and R/RMW bins of width 0.2.
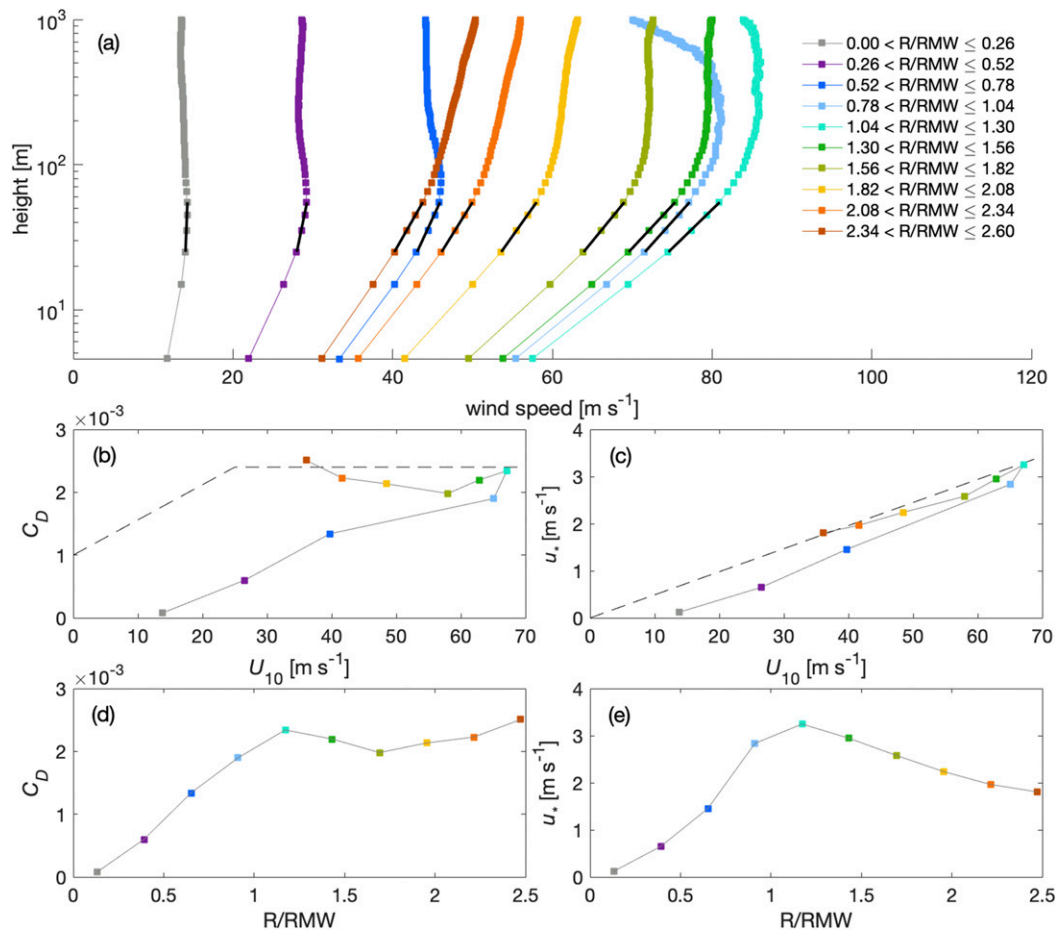
FIG. 10. (a) The mean wind profile measured by virtual sondes at various R/RMW ratios. The black lines show the logarithmic profile, fitted over a height range from 20 to 60 m. (b) The dependence of the retrieved C_D on U_{10}, with the dashed line showing the prescribed value in CM1. (c) The variation of u_* with U_{10}, with the dashed line indicating the prescribed relationship in CM1. (d) Dependence of C_D on R/RMW. (e) Dependence of u_* on R/RMW. The retrieved values shown in (b)–(e) are based on the profiles fitted over the height range 20–60 m.

itself, despite caveats which may exist in the realism of the simulated storm.

From the large number of virtual sondes (roughly 10^5), Fig. 9 shows the average composite of mean velocity as a function of radius and height, analogous to Fig. 1. As expected, the wind speed peaks at R/RMW ≈ 1, and occurs at roughly $z = 400$ m. The features in Fig. 9 are essentially the same as those discussed in Stern and Bryan (2018). The continuous rise in the height of the maximum wind (dashed line) indicates that far away from the RMW, the wind speed is monotonic with height through the first 2 km of the atmosphere, as expected under more horizontally homogeneous conditions. In that sense, we anticipate that at some radius the boundary layer flow should begin to better align with the assumptions underlying flux-profile theory (e.g., horizontal homogeneity, uniform geostrophic forcing), and that the predictions of u_* and C_D match the true values.

Figure 10 provides the mean profiles, as well as C_D and u_* estimates obtained from the virtual sondes. From Fig. 10a, it

appears that there is indeed a logarithmic layer persistent throughout the range of R/RMW, similar to the real sondes in Fig. 2a. In this particular simulation, the logarithmic region does not appear to extend beyond $z \approx 60$ m, and so the logarithmic fit is performed over the range $20 < z < 60$ m. The resulting C_D and u_* estimates in Figs. 10b and 10c, respectively, demonstrate very clearly that the flux-profile method successfully retrieves the true, prescribed values (dashed lines), but only when outside of the RMW. Beginning around R/RMW ≈ 1, the estimated values of C_D begin to underpredict compared to the prescribed value. A corresponding trend is seen in Fig. 10c for u_*. Inside the eye, the estimated values of C_D and u_* are unrealistically low compared to the known prescribed values.

Figures 10d and 10e present C_D and u_* as a function of R/RMW instead of U_{10}, and the strong radial dependence of both of these estimated quantities is apparent in the region near and inside R/RMW ≈ 1. When considering the real sondes, Fig. 3 does not display such an obvious trend near
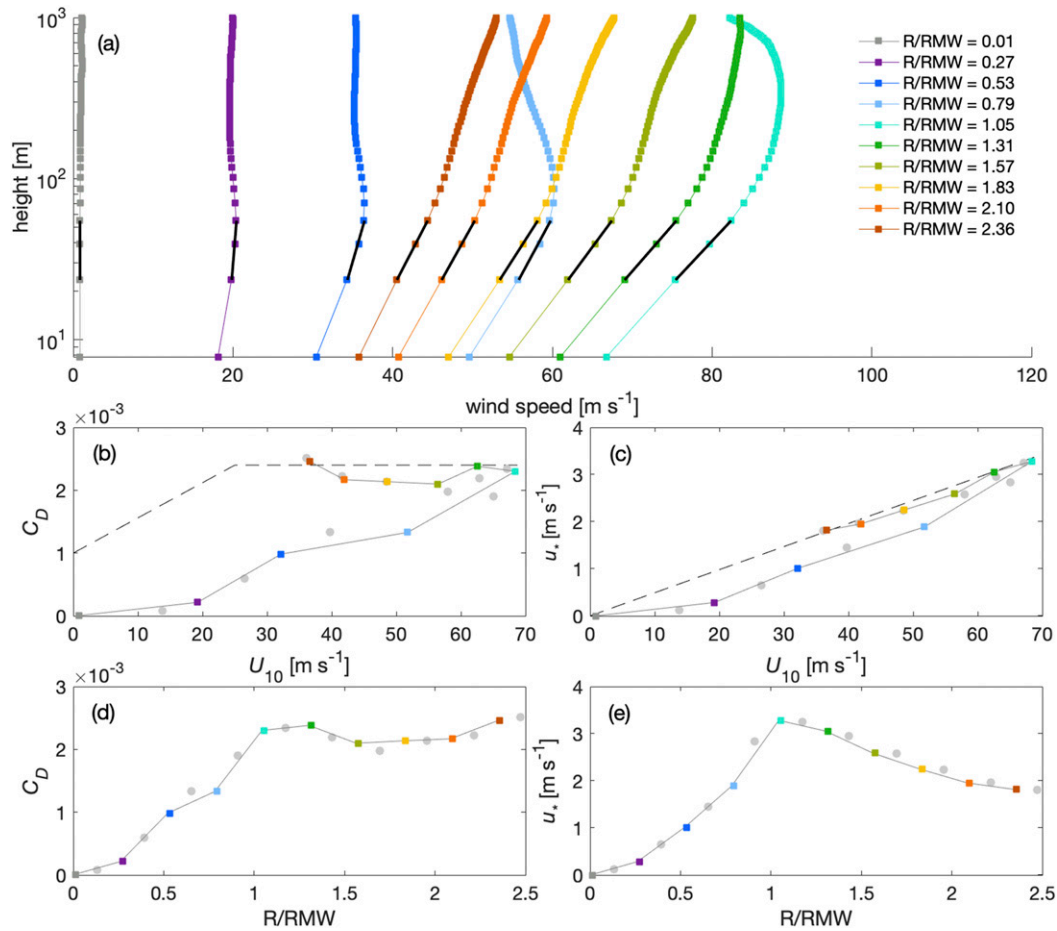
FIG. 11. (a) The azimuthally averaged wind profile at various distances from the storm center. The black lines show the logarithmic profile, fitted over a height range from 23 to 54 m. (b) The dependence of the retrieved C_D on U_{10}, with the dashed line showing the prescribed value in CM1. (c) The variation of u_* with U_{10}, with the dashed line indicating the prescribed relationship in CM1. (d) Dependence of C_D on R/RMW. (e) Dependence of u_* on R/RMW. The retrieved values shown in (b)–(e) are based on the profiles fitted over the height range 23–54 m, and the gray circles show the corresponding values from Fig. 10.

R/RMW ≈ 1, but the reason is straightforward. The virtual sondes not only are taken from a single storm with a clear, well-defined RMW, but the high number of virtual sondes allows for binning sondes into narrow R/RMW categories while still retaining adequate sample sizes. The real sondes, on the other hand, are being averaged over many storms, each with different size and intensity, and furthermore, we do not know the RMW for any given storm with the precision necessary to make a detailed, direct comparison. What this analysis suggests, ultimately, is that efforts to estimate u_* and C_D in the eye and eyewall are more likely to be underestimates, rather than overestimates, of the actual values.

One possible source of uncertainty in using dropsondes to construct mean velocity profiles, particularly in the context of employing the flux-profile method, is in the fact that sondes drift as they fall and therefore do not provide a strictly vertical profile (Stern and Bryan 2018; Kepert 2006). It is therefore instructive to perform the exact same analysis but on the true

vertical profiles obtained from the simulation computational grid. This is shown in Fig. 11, which provides azimuthally averaged velocity profiles at specific radii, as well as the C_D and u_* estimates from these.

When comparing Figs. 10 and 11, any differences are attributed to the drift, and potential biased sampling, of the virtual sondes as they measure the flow during their descent. The figures indicate, however, that the mean velocity profiles are very similar in shape, suggesting that the drift effect is minor. Over the height range where the profile data were used, the maximum azimuthal drift of the virtual sondes was 36°. Fitting over roughly the same height as for the virtual sondes (there are slight differences based on the grid levels) yields C_D and u_* estimates that are not only quantitatively similar, but have the same dependence on R/RMW. We thus conclude that the effects of sonde drift and the associated deviation from a true vertical profile is negligible, and postulate that the same is true for the observational sondes as well. Given that sonde drift

is likely larger in the azimuthal direction than in the radial direction, particularly in the eyewall, we argue that this is a reasonable conclusion.

The comparison of the flux-profile estimates to the known u_* and C_D from the virtual sondes first confirms that this procedure is capable of recovering the true surface stress and flux coefficients, sufficiently far from the RMW. What is required, however, is knowledge of the fitting range as well as an adequate sample size—both of which are available for the virtual sondes. What this analysis also shows is that the flux-profile method may not be applicable at or near the RMW. As argued elsewhere (Smith and Montgomery 2014), conditions near the RMW are quite far removed from the standard assumptions behind the Monin–Obukhov similarity theory and the logarithmic layer, and the logarithmic layer itself is restricted in height. A number of studies (Kepert 2001; Bryan et al. 2017) show that terms of the momentum transfer budget other than turbulent stress, especially including mean radial advection of azimuthal momentum as well as mean vertical transport, are dominant near the RMW, disrupting the notion of a constant stress layer which is linked to (though not synonymous with) the logarithmic layer. Despite observing a logarithmic velocity profile in both the real and virtual sondes near the RMW, these extra mechanisms of momentum transport perhaps unsurprisingly modify the relationship between the mean velocity and the surface stress, thereby possibly precluding accurate use of the flux-profile method under these conditions. The results in Fig. 10 suggest that these errors probably lead to underestimation, relative to the true value of C_D.

4. Conclusions

In this study we revisit the procedure of P03 for estimating the surface stress and drag coefficient at high winds by applying the flux-profile method to a large database of dropsondes. Our aim is to investigate in detail the behavior of C_D at high winds within the context of the limitations to the flux-profile method, and discuss the possibility that the decrease of C_D found at very high winds by P03 could result from an inherent bias in the method.

We originally hypothesized that the success of the flux-profile method would be a function of storm radius, due to the extra dynamics at play (radial pressure gradient and mean advection of angular momentum), and while appearing to be true in the virtual sondes that are near and in the hurricane eye, no such evidence is found in the observational sondes. These results do not conclusively rule this radial dependence out, however, simply because of large statistical uncertainty. The RMW cannot be known to the precision necessary to draw this conclusion, and other factors associated with the binning and averaging procedure induce a significant uncertainty. By randomly subsampling the full observational dataset, we see a wide spread in the prediction of C_D, to the point where even the sign of the C_D versus U_{10} slope at hurricane-force wind speeds cannot be determined with certainty. Of course there may even be reason to expect such variability, since there is growing evidence that C_D is not only a function of U_{10}, but other factors as well including waves (Hsu et al. 2019).

Furthermore, a few factors suggest that in addition to this uncertainty, there is reason to believe that the flux-profile method has an inherent low bias at the highest winds. These factors include the nonmonotonic profile of wind speed with height near the RMW, which leads to a monotonically decreasing estimate of u_* and C_D if the fitting height is increased. Also explored is the fact that the precise vertical location of the sonde is uncertain as well. By comparing the u_* to an independent dataset, adjustments to the geopotential height recorded by the dropsonde which improve the alignment between the u_* estimates also suggest that C_D would be underestimated. The tendency to underestimate u_* and C_D is also seen in the virtual sondes near and inside the RMW, where the estimated values can be compared to known quantities. Here, the balance of stresses is far removed from those assumed in traditional Monin–Obukhov similarity theory, so it is reasonable that despite the presence of a logarithmic mean velocity profile, the typical relationship between the velocity and surface stress would be disrupted.

Ultimately, there is reason to believe that the flux-profile method provides uncertain and possibly erroneously low values of C_D at the highest winds, and that the C_D versus U_{10} relationship does not actually exhibit a nonmonotonic peak. Since the failure of the flux-profile method appears to be linked to the storm-relative location, there is not necessarily a single wind speed above which one should expect an underprediction with this method, although a rough estimate based on Fig. 6 would put it around $35 \, \mathrm{m \, s^{-1}}$. More broadly, we also suggest that due to sample size and various sensitivities within the method itself, we are at the limit of how precise our estimates of the surface flux coefficients can be. While additional dropsonde measurements would improve this uncertainty, particularly at high winds, other methods of measuring fluxes, such as direct measurements using unmanned systems, likely represent the path forward for narrowing our uncertainty of air–sea exchange in tropical cyclones.

REFERENCES

Andreas, E. L., and K. A. Emanuel, 2001: Effects of sea spray on tropical cyclone intensity. *J. Atmos. Sci.*, **58**, 3741–3751, https://doi.org/10.1175/1520-0469(2001)058<3741:EOSSOT>2.0.CO;2.

——, J. B. Edson, E. C. Monahan, M. P. Rouault, and S. D. Smith, 1995: The spray contribution to net evaporation from the sea: A review of recent progress. *Bound.-Layer Meteor.*, **72**, 3–52, https://doi.org/10.1007/BF00712389.

——, L. Mahrt, and D. Vickers, 2012: A new drag relation for aerodynamically rough flow over the ocean. *J. Atmos. Sci.*, **69**, 2520–2537, https://doi.org/10.1175/JAS-D-11-0312.1.

Bao, J.-W., C. W. Fairall, S. A. Michelson, and L. Bianco, 2011: Parameterizations of sea-spray impact on the air–sea momentum and heat fluxes. *Mon. Wea. Rev.*, **139**, 3781–3797, https://doi.org/10.1175/MWR-D-11-00007.1.

Bell, M. M., M. T. Montgomery, and K. A. Emanuel, 2012: Air–sea enthalpy and momentum exchange at major hurricane wind speeds observed during CBLAST. *J. Atmos. Sci.*, **69**, 3197–3222, https://doi.org/10.1175/JAS-D-11-0276.1.

Bi, X., and Coauthors, 2015: Observed drag coefficients in high winds in the near offshore of the South China Sea. *J. Geophys. Res. Atmos.*, **120**, 6444–6459, https://doi.org/10.1002/2015JD023172.

Black, P. G., and Coauthors, 2007: Air–sea exchange in hurricanes: Synthesis of observations from the coupled boundary layer air–sea transfer experiment. *Bull. Amer. Meteor. Soc.*, **88**, 357–374, https://doi.org/10.1175/BAMS-88-3-357.

Bryan, G. H., 2012: Effects of surface exchange coefficients and turbulence length scales on the intensity and structure of numerically simulated hurricanes. *Mon. Wea. Rev.*, **140**, 1125–1143, https://doi.org/10.1175/MWR-D-11-00231.1.

——, and J. M. Fritsch, 2002: A benchmark simulation for moist nonhydrostatic numerical models. *Mon. Wea. Rev.*, **130**, 2917–2928, https://doi.org/10.1175/1520-0493(2002)130<2917:ABSFMN>2.0.CO;2.

——, and H. Morrison, 2012: Sensitivity of a simulated squall line to horizontal resolution and parameterization of microphysics. *Mon. Wea. Rev.*, **140**, 202–225, https://doi.org/10.1175/MWR-D-11-00046.1.

——, R. P. Worsnop, J. K. Lundquist, and J. A. Zhang, 2017: A simple method for simulating wind profiles in the boundary layer of tropical cyclones. *Bound.-Layer Meteor.*, **162**, 475–502, https://doi.org/10.1007/s10546-016-0207-0.

Cione, J. J., and Coauthors, 2020: Eye of the storm: Observing hurricanes with a small unmanned aircraft system. *Bull. Amer. Meteor. Soc.*, **101**, E186–E205, https://doi.org/10.1175/BAMS-D-19-0169.1.

Curcic, M., and B. K. Haus, 2020: Revised estimates of ocean surface drag in strong winds. *Geophys. Res. Lett.*, **47**, e2020GL087647, https://doi.org/10.1029/2020GL087647.

Demuth, J., M. DeMaria, and J. A. Knaff, 2006: Improvement of Advanced Microwave Sounding Unit tropical cyclone intensity and size estimation algorithms. *J. Appl. Meteor. Climatol.*, **45**, 1573–1581, https://doi.org/10.1175/JAM2429.1.

Donelan, M. A., B. K. Haus, N. Reul, W. J. Plant, M. Stiassnie, H. C. Graber, O. B. Brown, and E. S. Saltzman, 2004: On the limiting aerodynamic roughness of the ocean in very strong winds. *Geophys. Res. Lett.*, **31**, L18306, https://doi.org/10.1029/2004GL019460.

Eliassen, A., 1971: On the Ekman layer in a circular vortex. *J. Meteor. Soc. Japan*, **49A**, 784–789, https://doi.org/10.2151/jmsj1965.49A.0_784.

Emanuel, K. A., 1986: An air–sea interaction theory for tropical cyclones. Part I: Steady-state maintenance. *J. Atmos. Sci.*, **43**, 585–605, https://doi.org/10.1175/1520-0469(1986)043<0585:AASITF>2.0.CO;2.

——, 1995: Sensitivity of tropical cyclones to surface exchange coefficients and a revised steady-state model incorporating

eye dynamics. *J. Atmos. Sci.*, **52**, 3969–3976, https://doi.org/10.1175/1520-0469(1995)052<3969:SOTCTS>2.0.CO;2.

——, 2012: Self-stratification of tropical cyclone outflow. Part II: Implications for storm intensification. *J. Atmos. Sci.*, **69**, 988–996, https://doi.org/10.1175/JAS-D-11-0177.1.

Foster, R. C., 2009: Boundary-layer similarity under an axisymmetric, gradient wind vortex. *Bound.-Layer Meteor.*, **131**, 321–344, https://doi.org/10.1007/s10546-009-9379-1.

French, J. R., W. M. Drennan, J. A. Zhang, and P. G. Black, 2007: Turbulent fluxes in the hurricane boundary layer. Part I: Momentum flux. *J. Atmos. Sci.*, **64**, 1089–1102, https://doi.org/10.1175/JAS3887.1.

Green, B. W., and F. Zhang, 2014: Sensitivity of tropical cyclone simulations to parametric uncertainties in air–sea fluxes and implications for parameter estimation. *Mon. Wea. Rev.*, **142**, 2290–2308, https://doi.org/10.1175/MWR-D-13-00208.1.

Holthuijsen, L. H., M. D. Powell, and J. D. Pietrzak, 2012: Wind and waves in extreme hurricanes. *J. Geophys. Res.*, **117**, C09003, https://doi.org/10.1029/2012JC007983.

Hsu, J. Y., R. C. Lien, E. A. D'Asaro, and T. B. Sanford, 2017: Estimates of surface wind stress and drag coefficients in Typhoon Megi. *J. Phys. Oceanogr.*, **47**, 545–565, https://doi.org/10.1175/JPO-D-16-0069.1.

——, ——, ——, and ——, 2019: Scaling of drag coefficients under five tropical cyclones. *Geophys. Res. Lett.*, **46**, 3349–3358, https://doi.org/10.1029/2018GL081574.

Jarosz, E., D. A. Mitchell, D. W. Wang, and W. J. Teague, 2007: Bottom-up determination of air–sea momentum exchange under a major tropical cyclone. *Science*, **315**, 1707–1709, https://doi.org/10.1126/science.1136466.

Kepert, J. D., 2001: The dynamics of boundary layer jets within the tropical cyclone core. Part I: Linear theory. *J. Atmos. Sci.*, **58**, 2469–2484, https://doi.org/10.1175/1520-0469(2001)058<2469:TDOBLJ>2.0.CO;2.

——, 2006: Observed boundary layer wind structure and balance in the hurricane core. Part I: Hurricane Georges. *J. Atmos. Sci.*, **63**, 2169–2193, https://doi.org/10.1175/JAS3745.1.

Komori, S., K. Iwano, N. Takagaki, R. Onishi, R. Kurose, K. Takahashi, and N. Suzuki, 2018: Laboratory measurements of heat transfer and drag coefficients at extremely high wind speeds. *J. Phys. Oceanogr.*, **48**, 959–974, https://doi.org/10.1175/JPO-D-17-0243.1.

Kudryavtsev, V., B. Chapron, and V. K. Makin, 2014: Impact of wind waves on the air-sea fluxes: A coupled model. *J. Geophys. Res. Oceans*, **119**, 1217–1236, https://doi.org/10.1002/2013JC009412.

Large, W. G., and S. Pond, 1981: Open ocean momentum flux measurements in moderate to strong winds. *J. Phys. Oceanogr.*, **11**, 324–336, https://doi.org/10.1175/1520-0485(1981)011<0324:OOMFMI>2.0.CO;2.

Monin, A. S., and A. M. Yaglom, 1971: *Statistical Fluid Mechanics.* Vol. 1. Dover Publications, 769 pp.

Montgomery, M. T., R. K. Smith, and S. V. Nguyen, 2010: Sensitivity of tropical-cyclone models to the surface drag coefficient. *Quart. J. Roy. Meteor. Soc.*, **136**, 1945–1953, https://doi.org/10.1002/qj.702.

Potter, H., H. C. Graber, N. J. Williams, C. O. Collins, R. J. Ramos, and W. M. Drennan, 2015: In situ measurements of momentum fluxes in typhoons. *J. Atmos. Sci.*, **72**, 104–118, https://doi.org/10.1175/JAS-D-14-0025.1.

Powell, M. D., P. J. Vickery, and T. A. Reinhold, 2003: Reduced drag coefficient for high wind speeds in tropical cyclones. *Nature*, **422**, 279–283, https://doi.org/10.1038/nature01481.

Richter, D. H., and D. P. Stern, 2014: Evidence of spray-mediated air-sea enthalpy flux within tropical cyclones. *Geophys. Res. Lett.*, **41**, 2997–3003, https://doi.org/10.1002/2014GL059746.

——, R. Bohac, and D. P. Stern, 2016: An assessment of the flux profile method for determining air–sea momentum and enthalpy fluxes from dropsonde data in tropical cyclones. *J. Atmos. Sci.*, **73**, 2665–2682, https://doi.org/10.1175/JAS-D-15-0331.1.

Sanford, T. B., J. F. Price, and J. B. Girton, 2011: Upper-ocean response to Hurricane Frances (2004) observed by profiling EM-APEX floats. *J. Phys. Oceanogr.*, **41**, 1041–1056, https://doi.org/10.1175/2010JPO4313.1.

Smith, R. K., 1968: The surface boundary layer of a hurricane. *Tellus*, **20**, 473–484, https://doi.org/10.3402/tellusa.v20i3.10026.

——, and M. T. Montgomery, 2014: On the existence of the logarithmic surface layer in the inner core of hurricanes. *Quart. J. Roy. Meteor. Soc.*, **140**, 72–81, https://doi.org/10.1002/qj.2121.

Sparks, N., K. K. Hon, P. W. Chan, S. Wang, J. C. L. Chan, T. C. Lee, and R. Toumi, 2019: Aircraft observations of tropical cyclone boundary layer turbulence over the South China Sea. *J. Atmos. Sci.*, **76**, 3773–3783, https://doi.org/10.1175/JAS-D-19-0128.1.

Stern, D. P., and G. H. Bryan, 2018: Using simulated dropsondes to understand extreme updrafts and wind speeds in tropical cyclones. *Mon. Wea. Rev.*, **146**, 3901–3925, https://doi.org/10.1175/MWR-D-18-0041.1.

Takagaki, N., S. Komori, N. Suzuki, K. Iwano, T. Kuramoto, S. Shimada, R. Kurose, and K. Takahashi, 2012: Strong correlation between the drag coefficient and the shape of the wind sea spectrum over a broad range of wind speeds. *Geophys. Res. Lett.*, **39**, L23604, https://doi.org/10.1029/2012GL053988.

Tang, B., and K. Emanuel, 2012: A ventilation index for tropical cyclones. *Bull. Amer. Meteor. Soc.*, **93**, 1901–1912, https://doi.org/10.1175/BAMS-D-11-00165.1.

Tennekes, H., 1973: The logarithmic wind profile. *J. Atmos. Sci.*, **30**, 234–238, https://doi.org/10.1175/1520-0469(1973)030<0234:TLWP>2.0.CO;2.

Troitskaya, Y. I., D. A. Sergeev, A. A. Kandaurov, G. A. Baidakov, M. A. Vdovin, and V. I. Kazakov, 2012: Laboratory and theoretical modeling of air-sea momentum transfer under severe wind conditions. *J. Geophys. Res.*, **117**, C00J21, https://doi.org/10.1029/2011JC007778.

——, ——, M. Vdovin, A. Kandaurov, O. Ermakova, and N. Takagaki, 2020: A laboratory study of the effect of surface waves on heat and momentum transfer at high wind speeds. *J. Geophys. Res. Oceans*, **125**, e2020JC016276, https://doi.org/10.1029/2020JC016276.

Veron, F., 2015: Ocean spray. *Annu. Rev. Fluid Mech.*, **47**, 507–538, https://doi.org/10.1146/annurev-fluid-010814-014651.

Vickery, P. J., D. Wadhera, M. D. Powell, and Y. Chen, 2009: A hurricane boundary layer and wind field model for use in engineering applications. *J. Appl. Meteor. Climatol.*, **48**, 381–405, https://doi.org/10.1175/2008JAMC1841.1.

Vigh, J. L., E. G. Gilleland, C. L. Williams, N. M. Dorst, D. R. Chavas, J. M. Done, B. G. Brown, and G. J. Holland, 2020: TC-OBS: The Tropical Cyclone Observations-Based Structure Database, version 0.42. NCAR Research Applications Laboratory, accessed 21 April 2020, https://doi.org/10.5065/D6BC3X95.

Voermans, J. J., H. Rapizo, H. Ma, F. Qiao, and A. V. Babanin, 2019: Air–sea momentum fluxes during Tropical Cyclone Olwyn. *J. Phys. Oceanogr.*, **49**, 1369–1379, https://doi.org/10.1175/JPO-D-18-0261.1.

Wang, J., and Coauthors, 2015: A long-term, high-quality, high-vertical-resolution GPS dropsonde dataset for hurricane and other studies. *Bull. Amer. Meteor. Soc.*, **96**, 961–973, https://doi.org/10.1175/BAMS-D-13-00203.1.

Wang, Y., J. D. Kepert, and G. J. Holland, 2001: The effect of sea spray evaporation on tropical cyclone boundary layer structure and intensity. *Mon. Wea. Rev.*, **129**, 2481–2500, https://doi.org/10.1175/1520-0493(2001)129<2481:TEOSSE>2.0.CO;2.

Willoughby, H. E., and M. B. Chelmow, 1982: Objective determination of hurricane tracks from aircraft observations. *Mon. Wea. Rev.*, **110**, 1298–1305, https://doi.org/10.1175/1520-0493(1982)110<1298:ODOHTF>2.0.CO;2.

Zhang, J. A., F. D. Marks, M. T. Montgomery, and S. Lorsolo, 2011a: An estimation of turbulent characteristics in the low-level region of intense Hurricanes Allen (1980) and Hugo (1989). *Mon. Wea. Rev.*, **139**, 1447–1462, https://doi.org/10.1175/2010MWR3435.1.

——, R. F. Rogers, D. S. Nolan, and F. D. Marks, 2011b: On the characteristic height scales of the hurricane boundary layer. *Mon. Wea. Rev.*, **139**, 2523–2535, https://doi.org/10.1175/MWR-D-10-05017.1.

Zhao, Z., P. W. Chan, N. Wu, J. A. Zhang, and K. K. Hon, 2020: Aircraft observations of turbulence characteristics in the tropical cyclone boundary layer. *Bound.-Layer Meteor.*, **174**, 493–511, https://doi.org/10.1007/s10546-019-00487-8.